Original Research Article

Development of a pyrolysis model for oriented strand board: Part II—Thermal transport parameterization and bench-scale validation

Junhui Gong[1,2] (ID)**, Hongen Zhou[1], Hong Zhu[1,3], Conor G McCoy[1] and Stanislav I Stoliarov[1]**

Abstract

Oriented strand board is a widely used construction material responsible for a substantial portion of the fire load of many buildings. To accurately model oriented strand board fire response, kinetics and thermodynamics of its thermal decomposition and combustion were carefully characterized using milligram-scale testing in part 1 of this study. In the current work, Controlled Atmosphere Pyrolysis Apparatus II tests were performed on representative gram-sized oriented strand board samples at a range of radiant heat fluxes. An automated inverse analysis of the sample temperature data obtained in these tests was employed to determine the thermal conductivities of the undecomposed oriented strand board and condensed-phase products of its decomposition. A complete pyrolysis model was formulated for this material and used to predict the mass loss rates measured in the Controlled Atmosphere Pyrolysis Apparatus II experiments. These mass loss rate profiles were predicted well with the exception of the second mass loss rate peak observed at 65 kW m^{-2} of radiant heat flux, which was underpredicted. To further validate the model, cone calorimeter tests were performed on oriented strand board at 25 and 50 kW m^{-2} of radiant heat flux. The results of these tests, including both mass loss rate and heat release rate profiles, were predicted reasonably well by the model.

[1]Department of Fire Protection Engineering, University of Maryland, College Park, MD, USA
[2]College of Safety Science and Engineering, Nanjing Tech University, Nanjing, China
[3]State Key Laboratory of Fire Science, University of Science and Technology of China, Hefei, China

Corresponding author:
Junhui Gong, Department of Fire Protection Engineering, University of Maryland, College Park, MD 20742, USA.
Email: gjh9896@njtech.edu.cn

Introduction

Wood-based composites, including panel products, glued-laminated timber, structural composite lumber, and wood-nonwood composites, are extensively used for a number of structural and nonstructural applications ranging from panels for interior and exterior covering to furniture and support structures in buildings. The basic elements for these composites include fibers, particles, flakes, veneers, laminates, or lumber in a variety of sizes and shapes.[1] A promising advantage of these wood-based composites is that wood with localized defects (such as knots), wood recovered from construction waste or industrial manufacturing processes, small-diameter timber, forest residues, or exotic and invasive species can all be effectively utilized. Furthermore, homogeneity and the properties of the wood-based composites can be engineered and controlled to suit specific needs. Among all the conventional wood-based composites, four products—plywood, oriented strand board (OSB), particleboard, and fiberboard—are used the most.[1] They are manufactured primarily from wood (often 94% or more by mass) with only a few percent of resin and other additives. Bonding in these panels is provided by thermosetting adhesive resins, including phenol-formaldehyde, urea-formaldehyde, melamine-formaldehyde, isocyanate, and bio-based adhesives. Additives such as wax, preservatives, or fire retardants may also be used to achieve better weather resistance, longer service time, or improved fire response.

OSB is the focus of the current study. It is an engineered structural-use panel manufactured from thin wood strands bonded together with water-resistant resin. The wood strands typically have an aspect ratio (length divided by width) of at least 3. OSB panels are usually made up of three layers of strands, the outer faces having longer strands aligned in the long direction and a core layer that is counter aligned or laid randomly using smaller strands. Orientation of different layers of aligned strands gives OSB greater bending strength and stiffness in the oriented or aligned direction. Despite all these merits, OSB is combustible and relatively easy to ignite.[1] Therefore, its utilization in various building applications requires an engineering assessment of its impact on the probability and severity of fire.

Such assessment can be carried out by performing a set of computational fire dynamics simulations exploring a range of possible fire scenarios. The critical inputs required for these simulations are properties of OSB that define the rate of production of gaseous pyrolysis products in response to external heating. These property sets are commonly referred to as pyrolysis models. Development of a complete pyrolysis model requires a detailed thermal decomposition reaction scheme, reaction kinetics and thermodynamics, and parameters describing the heat and mass transfer in the condensed phase. While some analyses of OSB flammability and relevant properties are available in the literature,[2–6] a complete pyrolysis model of this material has not been formulated.

In part I of this study,[7] thermogravimetric analysis (TGA), differential scanning calorimetry (DSC), and microscale combustion calorimetry (MCC) were performed on representative milligram-sized OSB samples and analyzed using an automated inverse modeling to determine the thermal decomposition mechanism, kinetic parameters, heat capacities of OSB components, heats of decomposition reactions, and heats of combustion of gaseous pyrolyzates. In this work, information on kinetics and thermodynamics of the thermal
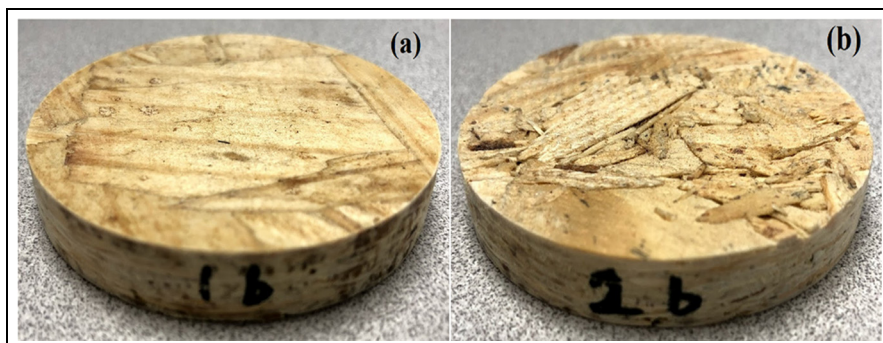
Figure 1. Photographs of OSB samples prepared for CAPA II tests: (a) smooth side facing up and (b) rough side facing up.

decomposition was utilized to inversely analyze solid temperature data collected in the radiation-driven Controlled Atmosphere Pyrolysis Apparatus II (CAPA II)[8] experiments performed on gram-sized OSB samples to determine the thermal transport properties and complete the pyrolysis model. The complete pyrolysis model was subsequently validated using a combination of mass loss rate (MLR) data collected in the CAPA tests and MLR and heat release rate (HRR) data collected in cone calorimetry tests[9] performed at a range of radiant heat flux settings.

Experimental

OSB samples

Georgia-Pacific Blue Ribbon PS2-10-compliant 2.44 m $\times$ 1.22 m $\times$ 0.011 m OSB sheets were purchased from a major U.S. distributor and used in part I[7] and current work. Disks with a diameter of 7 cm and 10 cm $\times$ 10 cm squares were cut from these sheets and used as samples for the CAPA II and cone calorimeter tests, respectively. All samples were conditioned in a desiccator in the presence of Drierite for at least 48 h prior to any analysis to minimize and control moisture content.

The bulk density of the dried OSB samples was measured at room temperature and found to vary across the sheet surface significantly, between 550 and 752 kg m^{-3}. The mean bulk density was determined to be 664 $\pm$ 56 kg m^{-3}, where the uncertainty was calculated as one standard deviation; these quantities were determined based on the analysis of over 60 samples. The sample thickness was 10.8 $\pm$ 0.1 mm; it varied little from sample to sample.

As indicated in Figure 1, the two sides of the OSB samples differed appreciably in appearance and texture. This difference was noted by labeling one side as "smooth" and the other side as "rough." The presence of this difference prompted an investigation into a potential variation in density through sample thickness. An approach similar to that employed by Ira and co-authors[2] was utilized, where thin layers of a sample were sanded off and the resulting changes in volume and mass were measured. This process was performed twice. The results of these measurements are summarized in Figure 2. These results indicate that the local density does vary with thickness and this variation is not symmetric with respect to the central
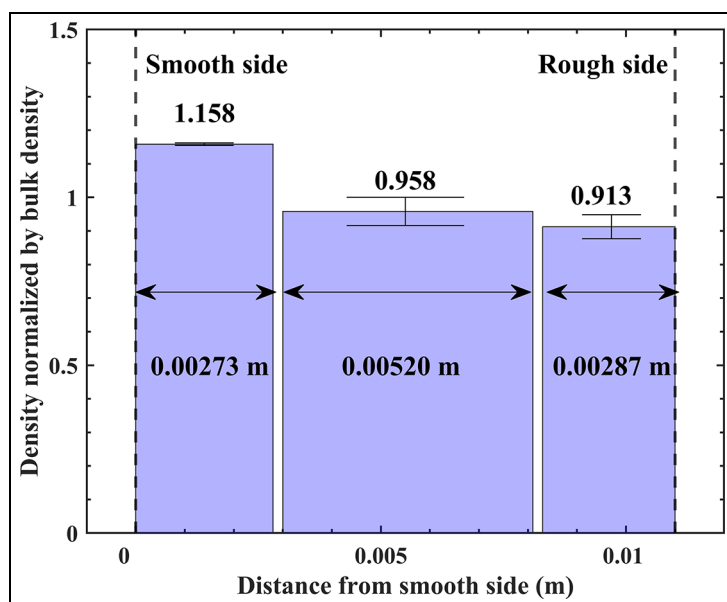
Figure 2. Fractional density variation across the thickness of the OSB sheets.

plane, as was hypothesized by Ira et al. Although the in-depth density variation is notable, it is not as large as the variation of the bulk density across the sheet surface. The impact of the density variations on the pyrolysis dynamics was examined during the pyrolysis model development, as discussed in detail in the subsequent sections.

CAPA II tests

CAPA II, shown in Figure 3, was designed to perform controlled-atmosphere, radiation-driven pyrolysis experiments on non-thermally thin samples. In this apparatus, the top surface of a disk-shaped sample is subjected to radiation from a temperature-controlled conical heater, while the temperature of the bottom of the sample is measured using a calibrated infrared (IR) camera. In addition to the bottom sample temperature, T_{bottom}, the mass and thickness profile of the sample are continuously monitored using a high-precision (1 mg resolution) balance and a high-definition video camera, respectively. The detailed description of the design and operation of this apparatus can be found in an earlier publication.[8]

The current measurements were performed in an anaerobic atmosphere (< 1 vol.% of O_2) obtained by purging the gasification chamber with 185 L min^{-1} of nitrogen. To ensure accurate T_{bottom} measurements, a thin copper foil painted with 0.92 broadband emissivity paint was firmly glued to the sample bottom with a small amount of high-temperature adhesive. The IR camera was focused on the foil through a gold mirror and the settings of the camera were adjusted to account for the mirror transmission loss. The side surface of the sample was thermally insulated with a ring cut out of Kaowool PM ceramic fiber board to minimize the lateral heat transfer. A fine (0.025 mm diameter bead) thermocouple was positioned inside the gasification chamber above the glass beads and was used to monitor the
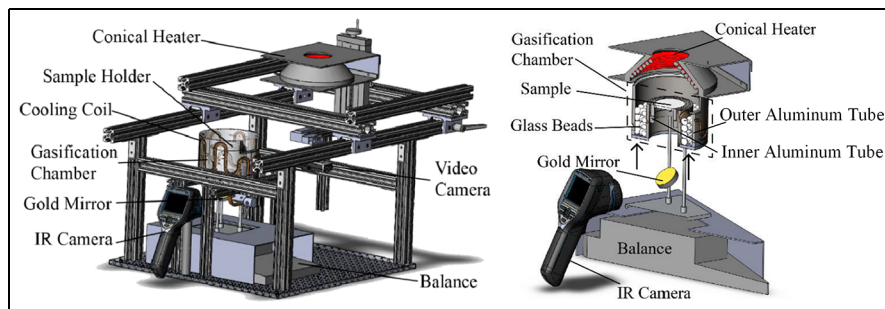
Figure 3. Schematic of the Controlled Atmosphere Pyrolysis Apparatus II (CAPA II).

temperature of nitrogen flowing over the top sample surface, T_{top}^e. This temperature was used to evaluate convective heat loss from this surface. Another thermocouple was attached to the inner surface of the gasification chamber facing the sample bottom. The temperature reading from this thermocouple, T_{bottom}^e, was used to compute convective and radiative heat feedback between the bottom sample surface and the environment.

The current experiments were carried out at 35 and 65 kW m^{-2} of radiant heat flux, which was set using a water-cooled Schmidt-Boelter heat flux transducer calibrated against a NIST-traceable reference. Four preliminary tests were performed at each heat flux to determine whether the sample orientation (smooth versus rough side exposed to the radiant heater) and/or bulk density variation significantly impact the results of the measurements. Subsequently, two final tests were performed at each heat flux and the results were used in the pyrolysis model for parameterization and validation.

Cone calorimeter tests

Cone calorimeter tests were performed in accordance with ASTM E1354.[9] The C-factor was calibrated daily and the calibration was verified by running a test on cast poly(methacrylate) and making sure that the measured heat of combustion matched published values. The OSB samples were mounted under the cone heater by wrapping the bottom and sides with aluminum foil and setting them atop two sheets of a 1.3-cm-thick Kaowool PM insulation board. No retainer frame was used. Ignition was accomplished via a spark igniter located 13 mm above the top sample surface. Three tests were performed at 25 kW m^{-2} of set radiant heat flux and another two tests were performed at 50 kW m^{-2}. Only two tests were performed at 50 kW m^{-2} because they were more repeatable. The OSB samples were found to smolder for extended periods of time after cessation of flaming. Therefore, the tests were stopped 100–200 s after flaming was over when no sensible MLR variation could be detected. Smoldering of the yielded residue is not the focus of this study, and the related data were not collected.

Modeling

The modeling was performed using the most recent version of the comprehensive pyrolysis solver ThermaKin, ThermaKin2Ds.[10] ThermaKin2Ds numerically solves mass and energy conservation equations for a condensed-phase object of arbitrary composition undergoing physical and chemical transformations. In part I of this study,[7] ThermaKin2Ds was used in

a thermally thin (zero-dimensional) mode to analyze the results of milligram-scale tests (TGA, DSC, and MCC) performed on OSB. In this work, ThermaKin2Ds was used in a one-dimensional mode to analyze and predict the results of CAPA II tests. The one-dimensional approximation was determined to be sufficient because the experimental data indicated that both T_{bottom} and sample thickness profiles remained nearly uniform in a radial direction for the duration of the CAPA II tests. Two one-dimensional ThermaKin simulations were used to model each cone calorimeter test, as further explained in section "Cone calorimeter modeling." The gas transfer coefficient was set at 2×10^{-5} m^2 s^{-1} for all gaseous decomposition products, which represents an unimpeded gas flow through the condensed phase. In both CAPA II and cone calorimeter models, the top sample surface was simulated to have no resistance to gas flow, while the bottom surface was set to be impenetrable to gas flow. All simulations were performed using 0.05 mm spatial discretization and 0.005 s time step. Increasing or decreasing these integration parameters by a factor of 2 did not produce any significant changes in the simulation results, indicating convergence. Simulations of CAPA II tests had a run time of 15–25 or 90–150 min depending on model complexity while simulations of cone calorimetry tests had a run time of 35–60 min on a single core of a PC.

CAPA II modeling

A previously developed expression describing dependence of the incident radiant heat flux on the location of the top sample surface was used in the CAPA II model to account for the heat flux variation with changes in the sample thickness and slight variation along the sample radius (which was averaged in this one-dimensional model). The convective heat loss from the top surface was calculated by using a previously determined convection Coefficient[8] of 7.2 W m^{-2} K^{-1}[8] and experimentally measured T_{top}^e, which evolution in time, t, was captured with:

$$T_{top}^e = T_1^e exp(t/\tau_1) + T_2^e exp(t/\tau_2) + T_{HFG} \tag{1}$$

where T_1^e, T_2^e, τ_1, and τ_2 are constants fitted to the experimental data, as shown in Figure 4, and T_{HFG} is the temperature of the heat flux transducer's cooling water. These constants are listed in Table 1. The bottom surface environmental temperature (T_{bottom}^e), which was used to compute convective and radiative heat feedback between to the bottom sample surface and the environment, was approximated by a piecewise linear expression:

$$T_{bottom}^e = \begin{cases} b_1 t + b_2, & when \quad t < t_c \\ b_3, & when \quad t \geq t_c \end{cases} \tag{2}$$

where b_1, b_2, b_3, and t_c are constants fitted to the experimental data, as shown in Figure 4. These constants are listed in Table 2. The convection coefficient used for the bottom surface, 4.0 W m^{-2} K^{-1}, was also determined in a previous study.[8]

As was determined in part I of this study,[7] the dried, undecomposed OSB consists of 1.9 wt.% of chemically bound water and 98.1 wt.% of organic constituents, referred to (cumulatively) as the OSB component. The decomposition reaction mechanism for the OSB is summarized in Table 3. This table also contains relevant reaction parameters including mass-based stoichiometric coefficients, pre-exponential factors (A), activation energies (E),
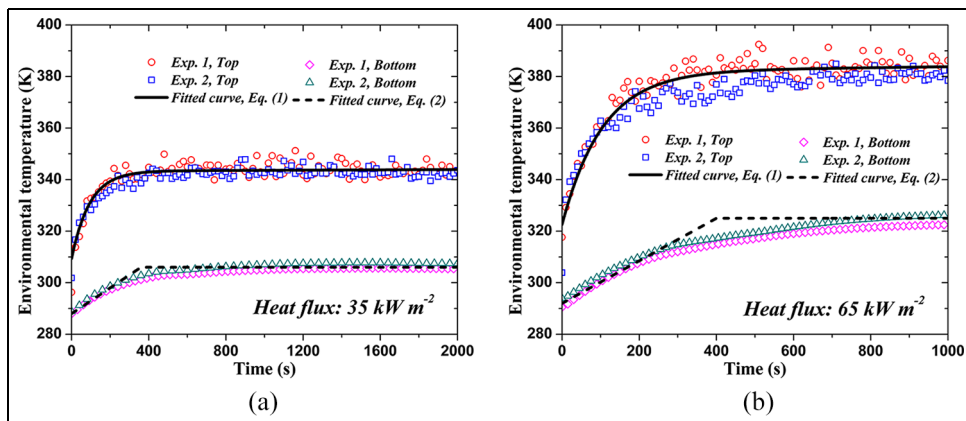
Figure 4. Measured and fitted environmental temperature histories observed in the CAPA II tests performed at (a) 35 and (b) 65 kW m^{-2} of set radiant heat flux.

Table 1. Parameters of equation (1) representing dependence of the top surface environmental temperature in CAPA II (T_{top}^e) on time.

Heat flux	35 kW m^{-2}	65 kW m^{-2}
T_1^e (K)	53.30	92.00
τ_1 (s)	1.82×10^6	5.18×10^4
T_2^e (K)	−33.97	−59.43
τ_2 (s)	−94.07	−105.15
T_{HFG} (K)	290	290

Table 2. Parameters of equation (2) representing dependence of the bottom surface environmental temperature in CAPA II (T_{bottom}^e) on time.

Heat flux	35 kW m^{-2}	65 kW m^{-2}
b_1 (K s^{-1})	0.05	0.0825
b_2 (K)	288	292
b_3 (K)	306	325
t_c (s)	360	400

and heats of reaction (h). Positive values of h correspond to exothermic reactions. All reactions used in this mechanism are of the first order. The heat capacities, C_p, of all condensed-phase components are listed in Table 4. The heat capacities of all gaseous OSB decomposition products were assumed to be equal to 2100 J kg^{-1} K^{-1}, which is the mean heat capacity of a collection of C1 to C8 hydrocarbons at a temperature of 600 K.[10] The heat capacity of the water vapor was obtained from the literature.[11] The heats of combustion, h_c, of the gaseous decomposition products are listed in Table 5. A, E, and stoichiometric coefficients were

Table 3. Reaction scheme and parameters obtained for the thermal decomposition of OSB (1.9 wt.% Water + 98.1 wt.% OSB component).[7]

Reaction #	Reaction equation	A (s^{-1})	E (J mol^{-1})	h (J kg^{-1})
1	Water → Water_vapor	1.55×10^4	4.35×10^4	-2.78×10^6
2	OSB → 0.72 OSB_int1 + 0.28 OSB_gas1	1.56×10^7	1.04×10^5	-6.82×10^3
3	OSB_int1 → 0.45 OSB_int2 + 0.55 OSB_gas2	2.65×10^{12}	1.74×10^5	-1.37×10^5
4	OSB_int2 → 0.77 OSB_int3 + 0.23 OSB_gas3	8.93×10^3	8.37×10^4	2.90×10^5
5	OSB_int3 → 0.77 Char + 0.23 OSB_gas4	4.40×10^{-1}	3.86×10^4	2.32×10^5

Positive values of h correspond to exothermic reactions.

Table 4. Heat capacities[7] and broadband emissivities of condensed-phase components of OSB.

Component	C_p (J kg^{-1} K^{-1})	Emissivity
Water	$5200 - 6.7\ T + 0.011\ T^2$	0.81
OSB	$-159 + 4.53\ T$	0.81
OSB_int1	$197 + 3.40\ T$	0.78
OSB_int2	$553 + 2.27\ T$	0.76
OSB_int3	$909 + 1.13\ T$	0.73
Char	1270	0.70

T is temperature in K.

determined from TGA; h and C_p were extracted from DSC results; and h_c was obtained from MCC experiments. The thermal decomposition model was able to predict MLR data of TGA, heat flow data of DSC, and peak heat release rate data of MCC tests within approximately 6%, 10%, and 5%, respectively.[7]

To complete the OSB pyrolysis model, its thermal transport properties were defined as follows. The OSB and its condensed-phase decomposition products were assumed to be opaque to thermal radiation (no in-depth absorption). Broadband emissivities were assigned using the data collected by Försth and Roos[12] for a similar engineered wood product, plywood. According to their measurements, the emissivity of plywood decreased from 0.81 to 0.70 as it underwent decomposition when exposed to a gray body radiation source at 1153 K. Consequently, the emissivities of the undecomposed OSB and the final residue (Char component) were assigned to be 0.81 and 0.70, respectively. The emissivities of the intermediate condensed-phase components were determined by linear interpolation. The emissivity of water was assumed to be the same as OSB. All emissivities are listed in Table 4.

Densities of the condensed-phase decomposition products were defined to capture changes in the sample thickness observed during the CAPA II tests. The gaseous components and water were assumed not to contribute to the sample volume. A detailed description of density parameterization is provided in section "Determination of thermal transport parameters." Thermal conductivities of the undecomposed OSB and its condensed decomposition products were determined through a Hill Climbing (HC) optimization algorithm implemented as a MATLAB script[13] coupled with ThermaKin2Ds to automate inverse analysis of the CAPA II data. A single goodness of fit criterion, GoF_T, was defined to quantify the convergence of the optimization:

Table 5. Heats of combustion of gaseous decomposition products of OSB.[7]

Component	h_c (J kg^{-1})
Water_vapor	0
OSB_gas1	1.25×10^7
OSB_gas2	1.52×10^7
OSB_gas3	1.15×10^7
OSB_gas4	0.75×10^7

Table 6. Flame heat feedback parameters of the two-zone model for cone calorimeter tests.[14]

	Center zone	Side zone
Radiative flame heat flux (kW m^{-2})	9.5	0
Convective flame heat flux (kW m^{-2})	$(3.7 \times 10^{-3})(2150 - T_{top})$	$(20 \times 10^{-3})(2150 - T_{top})$

T_{top} is the top sample surface temperature.

$$GoF_T = 1 - \sqrt{\frac{\sum_{i=1}^{N} \left(\frac{T_{bottom,i}^{model} - T_{bottom,i}}{T_{bottom,i}} \right)^2}{N}} \qquad (3)$$

where $T_{bottom,i}^{model}$ and $T_{bottom,i}$ are the simulated and measured bottom surface temperatures, respectively; and N is the total number of the experimental data points. A GoF_T of 1 implies a perfect fit.

Cone calorimeter modeling

The cone calorimeter modeling was performed using the OSB pyrolysis model which parameterization was completed through inverse analysis of the CAPA II tests. The top sample surface thermal boundary conditions were defined using a recently developed two-zone model.[14] A square area at the center of the sample, representing about 29% of the top surface, was defined as "Center zone." The rest of the sample top surface was defined as "Side zone." Two one-dimensional ThermaKin simulations, one for each zone, were run and the results were combined using surface-area-weighted contributions to compute the cone calorimeter MLR and HRR. The HRR was calculated by multiplying the mass production rate of each gaseous component by its heat of combustion, listed in Table 5, and adding them together.

The introduction of two zones was motivated by significant differences in the flame heat feedback (both in magnitude and nature) across the sample surface observed for a range of polymeric solids. The model of this flame heat feedback is summarized in Table 6. Flame ignition was assumed to take place once the gaseous fuel mass flux reached the magnitude corresponding to a critical value of HRR of 21 kW m^{-2}.[15] The convective losses from the top sample surface prior to ignition and radiative losses before and after ignition were also accounted for. The heat losses from the bottom sample surface to Kaowool PM insulation were modeled explicitly using its well-defined properties.[16]
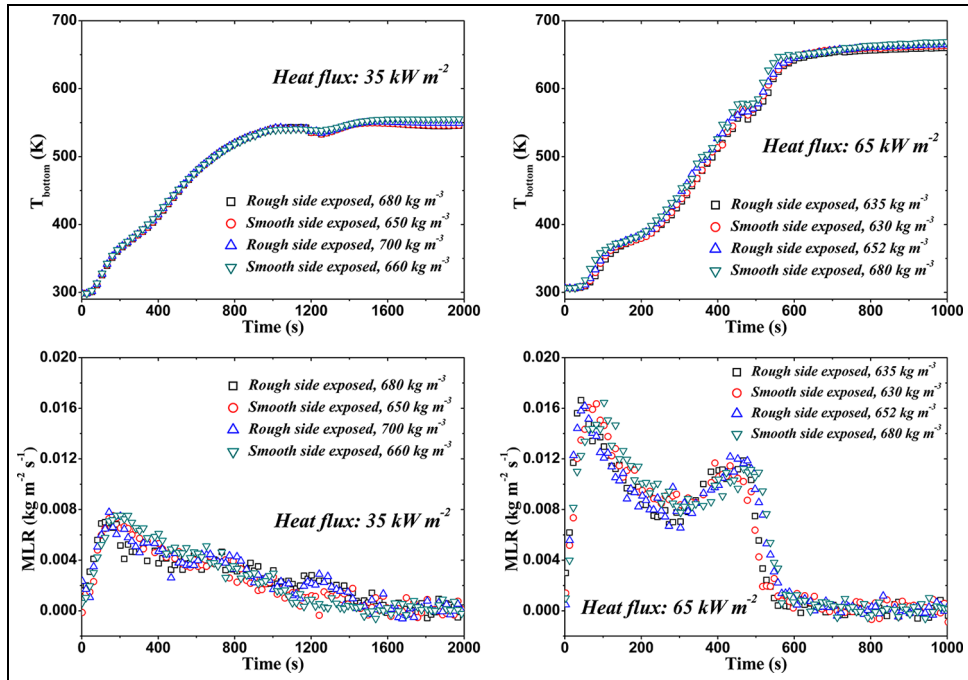
Figure 5. Results of CAPA II tests obtained for OSB samples of different bulk densities with either rough or smooth side of the sample facing the radiant heater.

Results and discussion

Effects of sample orientation and density

The results of preliminary CAPA II tests that were performed to determine whether the sample orientation (smooth versus rough side exposed to the radiant heater) and bulk density variation significantly impact the dynamics of pyrolysis are summarized in Figure 5. These results indicate that the sample orientation makes no significant difference. The density variation, roughly corresponding to one standard deviation, makes only a subtle difference. The second MLR peak observed at 65 kW m^{-2} shifts slightly to a later time with increasing density.

Determination of thermal transport parameters

For the final CAPA II tests performed at each heat flux, the samples were selected to have matching bulk densities, within 20 kg m^{-3} of each other. Also, for consistency, all final CAPA II tests were performed with the rough side of the sample facing the heater. The mean T_{bottom} data collected in the 65 kW m^{-2} tests were chosen as a target for the thermal conductivity optimization because the samples did not completely decompose in the 35 kW m^{-2} tests.

Two versions of the OSB pyrolysis model were formulated. In the first version, referred to as uniform density model, the undecomposed OSB sample was assumed to have a uniform density equal to the mean OSB sheet density of 664 kg m^{-3}. The densities of the condensed-

Table 7. Densities in kg m^{-3} of condensed-phase components of OSB.

Component	Uniform density model: OSB	Non-uniform density model: OSB1	Non-uniform density model: OSB2
OSB	652	800	550
OSB_int1	468	573	394
OSB_int2	184	226	156
OSB_int3	142	174	120
Char	108	133	91

phase decomposition products were subsequently adjusted to capture the experimentally measured sample thickness increase observed in the 65 kW m^{-2} CAPA II tests, which was to about 1.6 mm or 15% of the original sample thickness. These densities are listed in Table 7. Note that the density of the undecomposed OSB component is slightly below the mean density of the sheet because the OSB also contains 1.9 wt.% of water that contributes to mass but not volume of the sample, thus increasing its overall density.

The second version of the model, referred to as non-uniform density model, was developed to take into account variations in bulk sample density and local sample density across thickness. In this model, the undecomposed OSB was defined as a mixture two components, OSB1 and OSB2, with densities of 800 and 550 kg m^{-3}, respectively. Aside from the difference in density, these components had exactly the same physical and chemical properties. They decomposed through the same reaction mechanism (summarized in Table 3). The only difference was that the densities of the respective condensed-phase products were different to ensure that the thermal decomposition of either OSB1 or OSB2 reproduced the experimentally observed increase in the OSB thickness upon pyrolysis. These density values are also provided in Table 7. The sample was modeled as a three-layer composite with each layer featuring different initial mass fractions of OSB1 and OSB2. These mass fractions were selected to capture the measured density profile thorough thickness, shown in Figure 2, and match the mean bulk density of the samples used in the target experiments.

The thermal conductivities of all condensed-phase components were assumed to be independent of temperature to minimize the number of adjustable parameters. In the non-uniform density model, the corresponding OSB1- and OSB2-derived components were assumed to have the same thermal conductivities. The optimized T_{bottom} profiles are compared with the experimental data in Figure 6. The error bars in the experimental data were computed from their scatter as two standard deviations of the mean. Both models show a slight underprediction of the experimental T_{bottom} at the early stages of pyrolysis but, overall, capture the experimental data well. The resulting thermal conductivity values are summarized in Table 8 and are also quite similar between the models. The uncertainties in the thermal conductivities were estimated to be approximately 10%. They were determined by varying their values until model predicted T_{bottom} were just within the experimental error bars.

Pyrolysis model validation

The remaining CAPA II final test results, namely, the mean MLR data at both heat fluxes and the mean T_{bottom} data obtained at 35 kW m^{-2}, were used for the pyrolysis model validation. The uncertainties in these data were computed from their scatter as two standard
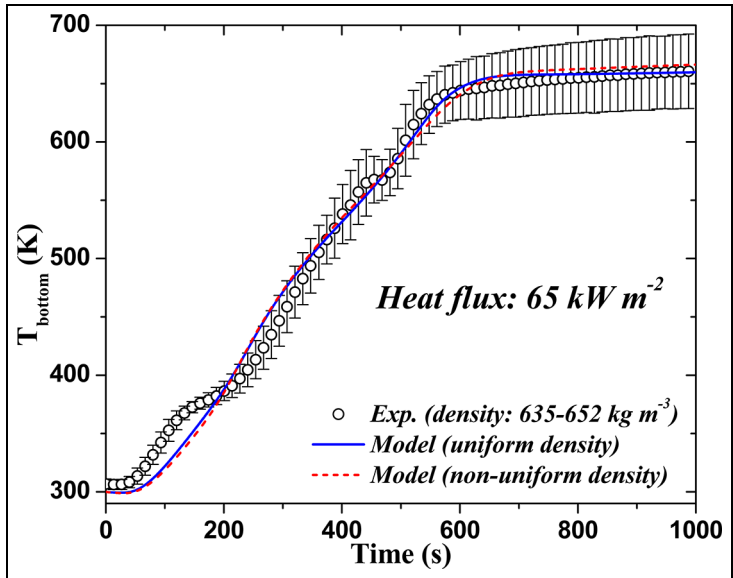
Figure 6. Experimental and modeled CAPA II bottom sample surface temperature profiles obtained at 65 kW m^{-2} of set radiant heat flux.

Table 8. Optimized thermal conductivities in W m^{-1} K^{-1} of condensed-phase components of OSB.

Component	Uniform density model	Non-uniform density model:OSB1 and OSB2
OSB	0.13	0.13
OSB_int1	0.06	0.10
OSB_int2	0.42	0.35
OSB_int3	0.39	0.39
Char	0.53	0.62

deviations of the mean. Comparisons between these data and model predictions are shown in Figures 7 and 8. Both uniform and non-uniform density models successfully capture the magnitudes of the main MLR peaks at both heat fluxes. Both models are also able to capture the T_{bottom} experimental data taken at 35 kW m^{-2} for the first 1000 s.

There are two main discrepancies: overestimation of experimental T_{bottom} after 1000 s at 35 kW m^{-2} and a significant (over 20 %) underestimation of the second (smaller) experimental MLR peak at 65 kW m^{-2}. Both discrepancies can be explained by an observed shrinkage of the samples in the radial direction over time. Figure 9 illustrates the extent of shrinkage seen for a 65 kW m^{-2} test. For the tests at 35 kW m^{-2}, shrinkage eventually resulted in partial decoupling of the sample from the copper foil. Consequently, measurements at later times underestimate T_{bottom}, making the model appear to overpredict T_{bottom}. For the tests at 65 kW m^{-2}, although samples remained in good contact with the copper foil during the test, greater shrinkage of the sample exposed the side sample surface to the radiation from the heater and thus produced additional heat flow into the sample which was not captured in the current simulations. The comparisons with the experimental data also
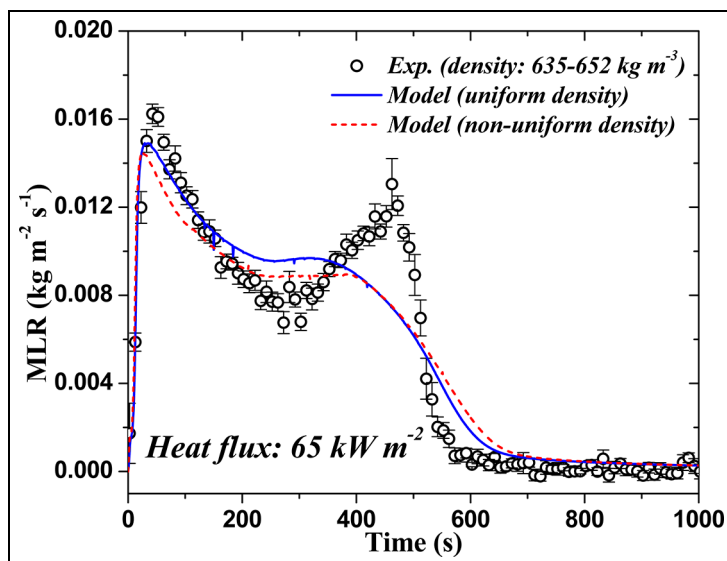
Figure 7. Experimental and modeled CAPA II mass loss rate profiles obtained at 65 kW m^{-2} of set radiant heat flux.
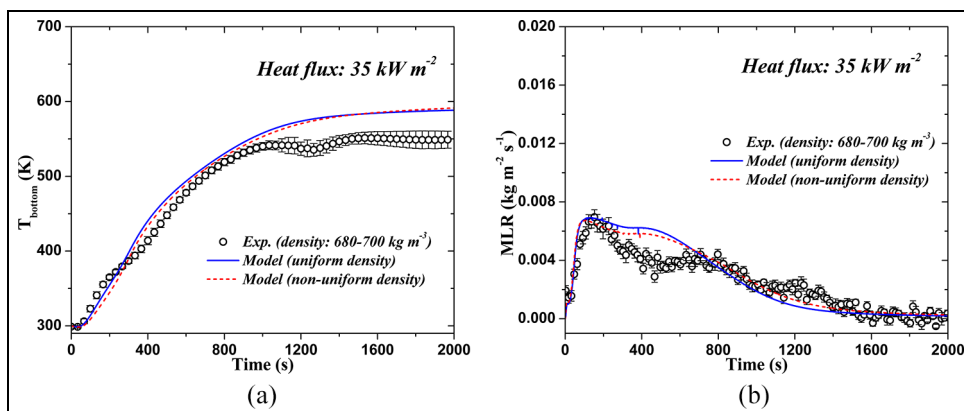

Figure 8. Experimental and modeled CAPA II (a) bottom sample surface temperature and (b) mass loss rate profiles obtained at 35 kW m^{-2} of set radiant heat flux.

indicate that the non-uniform density model, while notably more complex, does not provide any significant improvements in the accuracy of predictions. Therefore, only the simpler, uniform density model was used in the cone calorimeter test simulations since it presents a significant reduction in computational cost.

Modeling of cone calorimeter tests

The experimental cone calorimeter MLR and HRR obtained at 25 and 50 kW m^{-2} of radiant heat flux together with the model predictions (generated using the uniform density
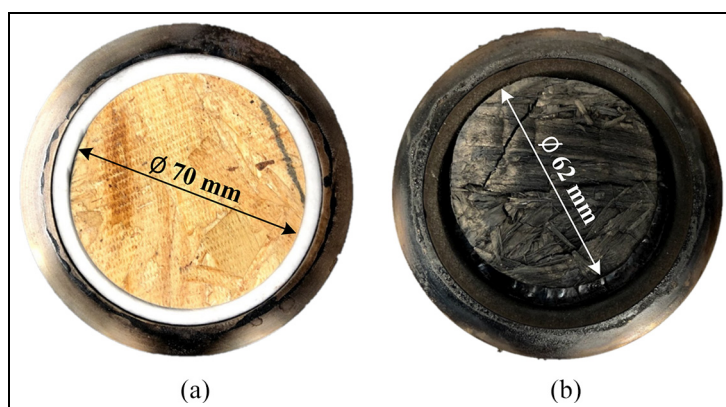
Figure 9. Snapshots of a CAPA II OSB sample (a) before and (b) after a test at 65 kW m^{-2}.
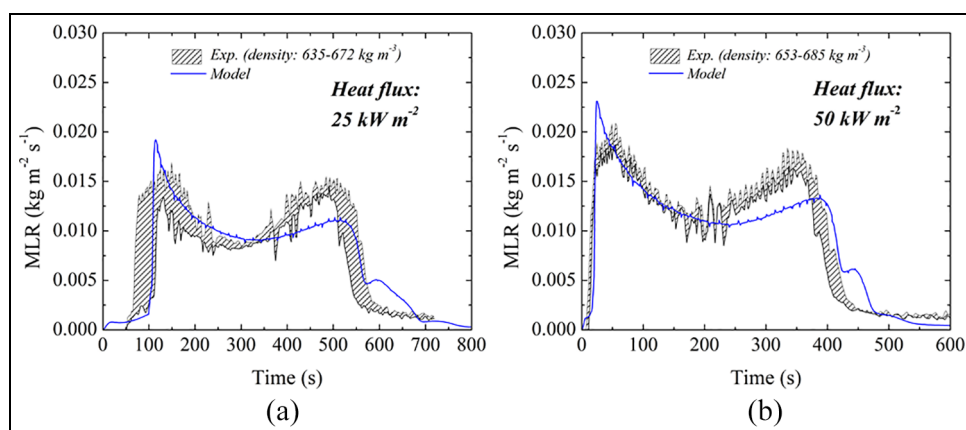

Figure 10. Comparison between measured and simulated MLR of OSB in cone calorimeter tests performed at (a) 25 kW m^{-2} and (b) 50 kW m^{-2} of set radiant heat flux. The shaded area represents the full range of the data obtained from repeated tests. The uniform density pyrolysis model was used in the simulations.

pyrolysis model) are shown in Figures 10 and 11. The experimental results are shown as a shaded area that represents the full range of the data obtained from repeated tests. Overall, the model predicts the experimental data well, especially taking into account that none of the cone calorimetry test results were used in the pyrolysis model calibration. The first MLR and HRR peaks are somewhat overpredicted by the model. This overprediction is more significant in the case of HRR, which may be explained by an incomplete combustion at the early stages of the cone calorimeter tests. The heats of combustion used in the model (and listed in Table 5) were obtained from MCC measurements, which force gaseous pyrolyzate combustion to completion.[17] Another possible explanation is that the response of the HRR measurement is not sufficiently fast to fully resolve these sharp peaks.

The second MLR peaks are somewhat underpredicted by the model but not as much as in the case of 65 kW m^{-2} CAPA II tests. The simulated second HRR peaks fall within the
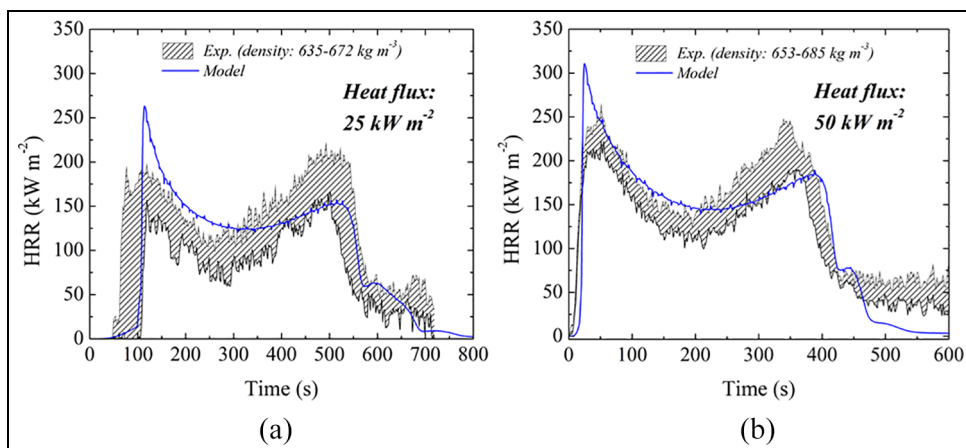
Figure 11. Comparison between measured and simulated HRR of OSB in cone calorimeter tests performed at (a) 25 kW m^{-2} and (b) 50 kW m^{-2} of set radiant heat flux. The shaded area represents the full range of the data obtained from repeated tests plus an additional 5% uncertainty associated with the orifice coefficient.[18] The uniform density pyrolysis model was used in the simulations.
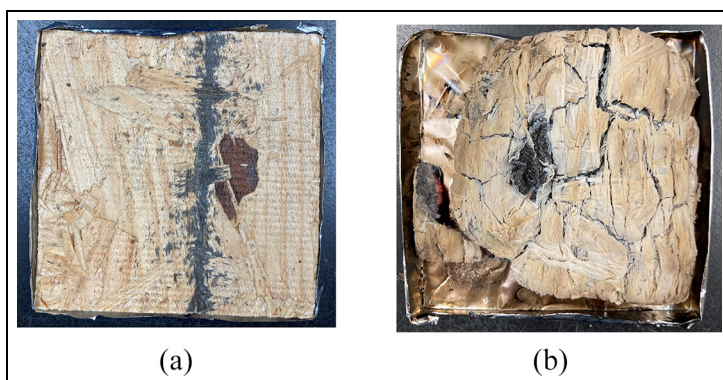

Figure 12. Snapshots of a cone calorimeter OSB sample (a) before and (b) after a test performed at 25 kW m^{-2}.

uncertainties of the corresponding experimental data at both heat fluxes. This improvement is likely due to the lack of significant sample shrinkage observed in the cone tests, perhaps because the bottom sample surface was not glued to the underlying foil, as was the case for the CAPA II tests. The cone samples do, however, exhibit cracking, as shown in Figure 12, which was not observed in the CAPA II tests. The cracking may produce increased radiation penetration into the sample and thus result in an increased second peak MLR.

Conclusion

In part I of this study,[7] a thermal decomposition model of OSB was formulated and parameterized using a set of TGA, DSC and MCC tests performed on mg-sized samples. This

model included a reaction mechanism, kinetic parameters, heats of reaction, heat capacities of condensed-phase OSB components and heats of combustion of gases produced during decomposition. In the current work, a set of CAPA II tests was performed on gram-sized samples at 35 and 65 kW m^{-2} of radiant heat flux. The bottom sample surface temperature profile obtained at 65 kW m^{-2} was inversely analyzed using the thermal decomposition model derived from the mg-scale tests to determine thermal conductivities of the condensed-phase components of OSB and complete the OSB pyrolysis model. The model was subsequently validated using the CAPA II MLR profiles obtained at 35 and 65 kW m^{-2} and bottom sample surface temperature profile obtained at 35 kW m^{-2}. In addition, standard cone calorimeter tests were conducted on the OSB at 25 and 50 kW m^{-2} of radiant heat flux and the results of these tests (both MLR and HRR) were successfully modeled using this pyrolysis model.

It was observed that the bulk density of OSB sheets varied significantly across the sheet surface. In addition, a notable variation in local density across sheet thickness was identified. The impact of these density variations on the pyrolysis dynamics was explored through a combination of experiments and modeling. It was determined that density variations do not have a significant impact and the version of the pyrolysis model utilizing an assumption of uniform density, which was set to be equal to the mean OSB sheet bulk density, provides sufficiently accurate predictions.

The pyrolysis model developed in this work is likely to be applicable to other OSB brands and thicknesses because they share similar composition and manufacturing process. The current model is not capable of simulating post-burning smoldering of the OSB residue. Considerable additional work will be required to extend this model to smoldering scenarios.

Declaration of conflicting interests

The author(s) declared no potential conflicts of interest with respect to the research, authorship, and/or publication of this article.

ORCID iD

Junhui Gong ⓘ https://orcid.org/0000-0003-0101-7448

References

1. Stark NM, Cai Z and Carll C. Wood-based composite materials panel products, glued-laminated timber, structural composite lumber, and wood-nonwood composite materials. In: *Wood handbook: wood as an engineering material*. Centennial ed. Madison, WI: Forest Products Laboratory, United States Department of Agriculture Forest Service, 2010, Pp. 11-1–11-28. https://www.fpl.fs.fed.us/documnts/fplgtr/fpl_gtr190.pdf

2. Ira J, Salek V, Jahoda M, et al. Thermal analysis and cone calorimeter study of engineered wood with an emphasis on fire modelling. *Fire Technol* 2020; 56: 1099–1132.

3. Hirle S and Balog K. The effect of the heat flux on the self-ignition of oriented strand board. *J Slovak Univ Technol* 2017; 25: 123–129.

4. White RH and Sumathipala K. Cone calorimeter tests of wood composites. In: *Proceedings of the Fire and Materials 2013 Conference*, San Francisco, CA, 28–30 January 2013, pp. 401–412. Gosport: Interscience Communications.

5. Ayrilmis N, Candan Z and White R. Physical, mechanical, and fire properties of oriented strand board with fire retardant treated veneers. *Holz Roh Werkst* 2007; 65: 449–458.

6. Mealy C, Boehmer H, Scheffey JL, et al. *Characterization of the flammability and thermal decomposition properties of aircraft skin composite materials and combustible surrogates*. Report no. DOT/FAA/TC-14/1, Federal Aviation Administration, Washington, DC, March 2014.

7. Gong J, Zhu H, Zhou H, et al. Development of a pyrolysis model for oriented strand board. Part I: kinetics and thermodynamics of the thermal decomposition. *J Fire Sci.* 2021; 39: 190–204.

8. Swann JD, Ding Y, McKinnon MB, et al. Controlled Atmosphere Pyrolysis Apparatus II (CAPA II): a new tool for analysis of pyrolysis of charring and intumescent polymers. *Fire Safety J* 2017; 91: 130–139.

9. ASTM International. ASTM E1354-17 Standard test method for heat and visible smoke release rates for materials and products using an oxygen consumption calorimeter. ASTM Stand 2017; 44: 2861–2869.

10. Swann JD, Ding Y and Stoliarov SI. Characterization of pyrolysis and combustion of rigid poly(vinyl chloride) using two-dimensional modeling. *Int J Heat Mass Tran* 2019; 132: 347–361.

11. McKinnon MB, Stoliarov SI and Witkowski A. Development of a pyrolysis model for corrugated cardboard. *Combust Flame* 2013; 160: 2595–2607.

12. Försth M and Roos A. Absorptivity and its dependence on heat source temperature and degree of thermal breakdown. *Fire Mater* 2010; 35: 285–301.

13. Fiola GJ, Chaudhari DM and Stoliarov SI. Comparison of pyrolysis properties of extruded and cast poly (methyl methacrylate). *Fire Safety J* 2021; 120: 103083.

14. McCoy CG, Tilles JL and Stoliarov SI. Empirical model of flame heat feedback for simulation of cone calorimetry. *Fire Safety J* 2019; 103: 38–48.

15. Lyon RE and Quintiere JG. Criteria for piloted ignition of combustible solids. *Combust Flame* 2007; 151: 551–559.

16. Leventon IT, Li J and Stoliarov SI. A flame spread simulation based on a comprehensive solid pyrolysis model coupled with a detailed empirical flame structure representation. *Combust Flame* 2015; 162: 3884–3895.

17. Lyon RE, Walters RN, Stoliarov SI, et al. *Principles and practice of microscale combustion calorimetry*. Report no. DOT/FAA/TC-12/53, Federal Aviation Administration, Washington, DC, April 2013.

18. Zhao L and Dembsey NA. Measurement uncertainty analysis for calorimetry apparatuses. *Fire Mater* 2007; 32: 1–26.

Author biographies

Junhui Gong is a visiting scholar at the University of Maryland and an associate professor at the Nanjing Tech University. He has a PhD in Fire Protection Engineering from the University of Science and Technology of China. His current research interests include pyrolysis and ignition of solid combustibles, numerical simulation of combustion, flame spread, leakage and dispersion of hydrogen in confined space.

Hongen Zhou has an MSc in Fire Protection Engineering at the University of Maryland. His Master's thesis focused on developing pyrolysis models for orientated strand board.

Hong Zhu is a visiting scholar at the University of Maryland and a post-doc at the University of Science and Technology of China. She has a PhD in Safety Science and Engineering from the University of Science and Technology of China. Her current research interests include pyrolysis, ignition, and flame spread of solid combustibles.

Conor McCoy is a PhD candidate with the University of Maryland. After graduation, he will begin a post-doc with UL Firefighter Safety Research Institute. His research interests include polymer flammability and oxidative pyrolysis.

Stanislav I. Stoliarov is a Professor of Fire Protection Engineering at the University of Maryland, College Park (USA). At Maryland, Stoliarov teaches a range of upper level undergraduate and graduate classes on the topics of fire dynamics, material flammability and fire modeling. His research group is engaged in a broad spectrum of activities focused on development of experimental and computational approaches to the analysis of flammability of polymeric and composite materials and fire safety of electrical and electronic devices.